RESEARCH ARTICLE

Correspondence to:
A. K. Naumann,
ann-kristin.naumann@mpimet.mpg.de

A Lagrangian drop model to study warm rain microphysical processes in shallow cumulus

Ann Kristin Naumann[1] and Axel Seifert[2]

[1]Max Planck Institute for Meteorology, Hamburg, Germany, [2]Hans-Ertel Centre for Weather Research, Deutscher Wetterdienst, Hamburg, Germany

Abstract In this study, we introduce a Lagrangian drop (LD) model to study warm rain microphysical processes in shallow cumulus. The approach combines Large-Eddy Simulations (LES) including a bulk microphysics parameterization with an LD model for raindrop growth. The LD model is one-way coupled with the Eulerian LES and represents all relevant rain microphysical processes such as evaporation, accretion, and selfcollection among LDs as well as dynamical effects such as sedimentation and inertia. To test whether the LD model is fit for purpose, a sensitivity study for isolated shallow cumulus clouds is conducted. We show that the surface precipitation rate and the development of the raindrop size distribution are sensitive to the treatment of selfcollection in the LD model. Some uncertainty remains for the contribution of the subgrid-scale turbulence to the relative velocity difference of a pair of LDs, which appears as a factor in the collision kernel. Sensitivities to other model parameters such as the initial multiplicity or the initial mass distribution are small. Overall, sensitivities of the LD model are small compared to the uncertainties in the assumptions of the bulk rain microphysics scheme, and the LD model is well suited for particle-based studies of raindrop growth and dynamics. This opens up the opportunity to study effects like recirculation, deviations from terminal fall velocity and other microphysical phenomena that so far were not accessible for bin, bulk, or parcel models.

1. Introduction

In atmospheric modeling, microphysical processes are traditionally parameterized on Eulerian grids either using bulk schemes or (potentially more accurate) bin schemes. On a microphysical process level, a Lagrangian approach is the most natural framework to study cloud droplet and raindrop development. Recently, the superdroplet method has been introduced to study cloud droplet behavior on a particle-based level and on domain sizes of a few kilometers [*Andrejczuk et al.*, 2008, 2010; *Shima et al.*, 2009; *Riechelmann et al.*, 2012]. Because cloud droplets are typically orders of magnitude more numerous than raindrops, those studies focus their computational resources mostly on cloud droplet behavior and an adequate representation of the tail of the drop size distribution, which is decisive for precipitation characteristics, is challenging. In this paper, we introduce a Lagrangian drop (LD) model that focuses on the raindrop phase and that targets specifically the warm rain microphysical processes and the growth history of raindrops after the initial formation of drizzle drops.

Warm rain bulk microphysics parameterizations usually distinguish between two hydrometeor classes: cloud droplets and raindrops [*Kessler*, 1969; *Beheng*, 1994] (for a triclass parameterization, see, e.g., *Sant et al.* [2013]). While the precise separation value in terms of drop radius or mass may differ between the studies, the cloud droplet class is generally defined such that the sedimentation velocity is negligible and cloud droplets are assumed to evaporate immediately when they encounter unsaturated air. For raindrops in contrast, condensational growth is neglected because collision-coalescence—both with cloud droplets and among raindrops—is the dominant growth mechanism. Also, raindrops do not behave like massless particles but have a mass-dependent sedimentation velocity and experience inertial effects.

To describe the cloud droplet and the raindrop development in space and time, bulk schemes assume that the cloud droplet size distribution and the raindrop size distribution (RSD) in a model grid box can be described well by a family of distributions with few free parameters. Changes in the RSD due to microphysical processes are then formulated as changes in the moments of the RSD. The different moments of the RSD have different sedimentation velocities, which in higher moment schemes generally allows for a

representation of gravitational sorting but is also known to produce too excessive sorting and even the occurrence of shock waves [*Wacker and Seifert*, 2001; *Mansell*, 2010; *Milbrandt and McTaggart-Cowan*, 2010].

In bin schemes, the drop size distribution in each model grid box is discretized in a (large) number of size bins, and the temporal development of the number of drops in each bin is calculated for each bin separately. Therefore, no artificial distinction between cloud droplets and raindrops is needed and (provided that the number of bins is high) the shape of the drop size distribution can evolve freely. Bin schemes are, however, known to encounter diffusion among bins and across grid box boundaries [*Stevens et al.*, 1996], which hinders a correct representation of important processes such as sedimentation. Another limitation of the bin schemes is that all particles in a bin have identical properties, e.g., fall speeds. This makes it difficult to study inertial effects or the history of raindrops.

In the LD model, we use the distinction between cloud droplets and raindrops from the bulk approach. We run a Large-Eddy Simulation (LES) model with a conventional two-moment bulk microphysics scheme that simulates both the cloud droplet and the raindrop phase [*Stevens and Seifert*, 2008]. In addition, the LD model also simulates the raindrop phase of the drop development but is run without feedbacks on the Eulerian LES fields. The RSD in the LD model is not restricted but each LD follows its own trajectory and size evolution driven by the time-dependent, thermodynamical background fields of the Eulerian LES. By allowing for subgrid-scale positions of the LDs within the Eulerian grid, also sedimentation and gravitational sorting are considered inherently.

We intend the LD model to be used as a tool to understand warm rain microphysical processes in shallow cumulus on a particle-based level. The LD model is suited to investigate a range of questions such as the effect of subcloud layer evaporation on the RSD, the importance of "lucky raindrops" for the formation of surface precipitation [*Magaritz et al.*, 2009] or the role of a subsiding shell for the growth history of raindrops in shallow cumulus [*Heus and Jonker*, 2008]. In this study, we test whether a particle-based model can be used to investigate these questions, i.e., whether the LD model is fit for purpose. To do this, we critically examine the assumptions made in the particle-based approach and attempt to quantify the uncertainties of the LD model. Such a quantification of the uncertainties of the introduced LD model is an essential prerequisite before the method can be applied to specific research questions such as those outlined above.

Several modifications of the LD model are conceivable to further broaden the scope of the method. For instance, the implementation of collisional raindrop breakup allows for the simulation of more heavily precipitating clouds and a detailed investigation of the effect of raindrop breakup on the RSD. Another application is the fragmentation of freezing raindrops to quantify their effect on the glaciation of cumulus cloud tops [*Rangno*, 2008].

The rest of the paper is structured as follows: in section 2, we shortly describe the LES model and the model setup for a test case of lightly precipitating shallow cumulus. We then introduce the LD model in section 3, in particular, the initialization of the LDs, the calculation of their trajectories, and the growth and shrinking mechanisms—accretion, selfcollection, and evaporation. In that section, we also briefly mention sensitivities to choices of model parameters from the test case setup that are found to be small. In section 4, we focus on those sensitivities to model assumptions that are relatively large and require a more detailed discussion: inertia, the subgrid-scale contribution of the fluid velocity, and their effects on the selfcollection rate. In section 5, we set the sensitivities of the LD model in context to uncertainties in the bulk microphysics parameterization. Finally, in section 6, we give some concluding remarks.

2. Test Case Description

2.1. Large Eddy Simulation

We use the University of California, Los Angeles LES (UCLA-LES) [*Stevens et al.*, 2005; *Stevens*, 2007] with a third-order Runge-Kutta scheme for time stepping. Prognostic equations are solved for the three components of the velocity, the total water mixing ratio, the liquid water potential temperature, the mass mixing ratio of rainwater, and the mass-specific number of raindrops. Warm cloud and rain microphysical processes are parameterized by the two-moment bulk microphysics scheme of *Seifert and Beheng* [2001] with a diagnostic shape parameter [*Seifert*, 2008] and a fixed cloud droplet density. We adjusted the density correction

Table 1. Characteristic Properties of Cloud A and Cloud B[a]

	t_{cloud} (min)	A_{max} (km^2)	LWP (g/m^2)	RWP (g/m^2)	z_{base} (m)	$z_{top,max}$ (m)
Cloud A	45	3.3	99	7.1	600	2500
Cloud B	55	2.4	94	5.7	650	2000

[a]t_{cloud}—cloud lifetime, A_{max}—maximum cloud area, LWP—mean in-cloud liquid cloud water path, RWP—mean in-cloud rainwater path, z_{base}—mean cloud base height, and $z_{top,max}$—maximum cloud top height.

exponent to 0.35 to better fit the behavior of small raindrops (see discussion in the Appendix A). Subgrid-scale fluxes are modeled with the Smagorinsky-Lilly model.

2.2. Case Setup

We use two variants of a case study of shallow cumulus over the ocean (Rain In Cumulus over the Ocean, RICO) [see *Rauber et al.*, 2007]. For the standard RICO simulation, the initial profiles and the large-scale forcing are described by *van Zanten et al.* [2011]. The moist RICO case differs from the standard setup only by a moister initial profile and was first used by *Stevens and Seifert* [2008]. For large domains, this moister setup results in a higher rain rate, which is both a result of and also a cause for mesoscale organization [*Seifert and Heus*, 2013]. We choose a much smaller domain size of 3.2 km in both horizontal directions. This has the advantage that there is basically a single cloud in the whole domain at one time, which allows us to isolate the behavior of an individual cloud.

We use a vertical domain size of 3.2 and 4.0 km for the standard and moist RICO setup, respectively, and a grid spacing of 25 m in all spatial directions for both setups. The time step is 1 s. The Eulerian model is run for 24 and 17 h for the standard and moist RICO setup, respectively. We then select the cloud that develops the most bulk rainwater for each run. Over the course of the lifetime of those two clouds (each 1.5 h), we let the model run again including the LDs and output the LD properties with a temporal resolution of 15 s. In the following, we refer to the cloud selected from the standard RICO setup as cloud A and to the cloud selected from the moist RICO setup as cloud B. We do not claim that cloud A (B) is more representative for drier (moister) environmental conditions but the two selected clouds should be seen as different realizations of shallow cumulus convection from slightly different environmental conditions. Some characteristic properties of the two clouds are given in Table 1. Overall, cloud B has a longer lifetime than cloud A and shows features of pulsating growth [*Heus et al.*, 2009] while the development of cloud A is characterized by a single but stronger updraft.

3. Lagrangian Drop Model

The LD method used here is based on the superdroplet approach [*Andrejczuk et al.*, 2008, 2010; *Shima et al.*, 2009; *Riechelmann et al.*, 2012], but adapted to focus on the raindrop distribution by considering basically two differences: first, instead of modeling the whole lifecycle of drops from their nucleation via a cloud droplet phase until a few of them eventually reach raindrop size, we simulate the raindrop phase only. By avoiding nucleation and cloud droplet growth processes for the LDs, (computational) resources are concentrated on the raindrop phase, which is very effective because cloud droplets are typically several orders of magnitude more numerous than raindrops.

A second major difference to the superdroplet method is that we do not use a two-way coupling of the LDs to the Eulerian model. The LD model uses the data from the Eulerian LES as input but is not coupled back to the Eulerian model. The Eulerian LES is run including all microphysics, especially also including the rain microphysics. Such a one-way coupling poses limitations on the usage of the LD model because differences in the rainwater fields of the bulk microphysics and the LD model result from the different formulations of microphysical processes and may lead to inconsistencies. In our simulations, the differences between the rainwater fields are small and hence a one-way coupling is appropriate here. Moreover, the one-way coupling allows for a meaningful comparison of the bulk rain microphysics and the LD statistics because the bulk rain microphysics and the LD model are forced by the same dynamical and thermodynamical fields. The limitations and advantages of comparing two parameterizations of which the first is fully coupled and the second is one-way coupled have recently been discussed by *Grabowski* [2014].

Table 2. Accumulated Surface Precipitation (R) and Slope of the RSD (Λ) from the Control Runs and Sensitivity Runs for the LD Model and the Bulk Rain Microphysics Scheme[a]

		Cloud A		Cloud B	
		R	Λ (mm^{-1})	R	Λ (mm^{-1})
c	Control run	679 kg	14.8	3925 kg	12.2
	Bulk: Control run	166%	21.3	63%	21.3
1	$\xi_0 = 1 \times 10^9$	97%	14.7	104%	12.9
1*	$\xi_0 = 1 \times 10^9$	108%	13.9	119%	11.3
c	Control run, $\xi_0 = 5 \times 10^8$	100%	14.8	100%	12.2
c*	$\xi_0 = 5 \times 10^8$	110%	13.8	111%	11.6
2	$\xi_0 = 2.5 \times 10^8$	127%	14.1	118%	12.0
2*	$\xi_0 = 2.5 \times 10^8$	118%	14.1	105%	12.6
3	$\xi_0 = 1.25 \times 10^8$	123%	14.3	108%	12.0
3*	$\xi_0 = 1.25 \times 10^8$	113%	14.6	114%	12.2
4	Initial mass distr. linear decr.	84%	14.8	95%	11.1
5	Initial mass distr. delta fct.	44%	15.9	71%	12.8
6	$r_{min} = 20~\mu m$	102%	14.6	116%	12.4
7	Selfcollection: vert. vel.	21%	18.3	79%	12.7
8	Selfcollection: S09	118%	14.2	112%	11.7
9	No selfcollection	0%	29.0	26%	14.3
10	Selfcollection: $E_c = 1$	1022%	8.2	155%	10.4
11	Traj.: no sgs vel.	55%	15.2	74%	13.6
12	Traj.: no inertia	120%	14.0	110%	11.0
I	Bulk: RSD: MY05	3128%	10.2	502%	11.3
II	Bulk: RSD: $\mu = 1$	7084%	7.6	847%	9.0
III	Bulk: RSD: $\mu = 10$	2%	36.7	3%	38.2
IV	Bulk: $n_c = 35 \times 10^6$ m^{-3}	625%	20.5	225%	22.1
V	Bulk: $n_c = 105 \times 10^6$ m^{-3}	33%	21.5	3%	20.3
13	$n_c = 35 \times 10^6$ m^{-3}	1978%	10.5	613%	9.5
14	$n_c = 105 \times 10^6$ m^{-3}	1%	18.1	8%	12.4

[a]For the sensitivity runs of the LD model and the bulk scheme, the accumulated surface precipitation is given as percentage of the LD control run. Sensitivity runs with a different random seed for the LD model are marked with asterisk. Sensitivity runs 7–12 are discussed in section 4. Sensitivity runs I–V, 13 and 14 are discussed in section 5.

To retrieve the properties of the ambient air of an LD, trilinear interpolation from the Eulerian grid to the subgrid-scale position of the LD is used for the liquid water potential temperature, the total water mixing ratio, the pressure, the subgrid-scale velocity variance, and the three components of the resolved fluid velocity. All derived variables such as the subsaturation for the calculation of evaporation are determined at the particle position from those interpolated variables.

To explore the sensitivities of the LD model to different model parameters, we ran several additional simulations each differing from the control run by one model parameter. The results are summarized in Table 2, which shows the accumulated surface precipitation for the whole domain and the whole simulation time, and the slope of the RSD after 30 min simulation time for cloud A and for cloud B. The slope of the RSD, Λ, is fitted for all LDs in the domain with a diameter $D > 200~\mu m$ to an exponential function: $RSD(D) = N_0 \exp(-\Lambda D)$ [*Marshall and Palmer*, 1948]. In the following, we will only briefly mention sensitivities due to the choice of model parameters that are rather small (sensitivity runs 1–6), and discuss model choices that have a stronger impact on the accumulated surface precipitation and on the RSD in section 4 in more detail (sensitivity runs 7–12).

We adapt the concept of multiplicity from the superdroplet method, i.e., one LD represents a multiplicity of raindrops of the same size. While the initial multiplicity of an LD is fixed for each run, during the LD's life-cycle, the multiplicity is allowed to change when collision-coalescence takes place. For the control run, we choose an initial multiplicity of $\xi_0 = 5 \times 10^8$. When increasing and decreasing the initial multiplicity (sensitivity runs 1–3 in Table 2), the slope of the RSD varies only slightly for cloud A and cloud B. The accumulated surface precipitation varies up to 30% for cloud A and up to 20% for the overall less sensitive cloud B.

For the initialization of the LDs (section 3.1) and for the selfcollection among the LDs (section 3.4), a Monte-Carlo sampling is applied. Sensitivity runs performed with a different initial seed for the Monte-Carlo processes (sensitivity runs with asterisk in Table 2) show deviations in the accumulated surface precipitation and the RSD of a similar magnitude as for the different initial multiplicities. Compared to other uncertainties,

e.g., in the treatment of selfcollection (sensitivity runs 7–10), the differences in the accumulated surface precipitation and the slope of the RSD are rather small for different initial multiplicities in the range considered here and for different random seeds. For a field of clouds, we expect the overall sensitivities to be smaller than the sensitivities for the isolated clouds shown here.

The initialization of the LDs, the calculation of their trajectory, which includes inertial effects and the influence of the subgrid-scale velocity, and their mass change due to evaporation, accretion, and selfcollection are described in more detail below. In the end, some details of the technical implementation of the LD model are outlined.

3.1. Initialization

The LDs are initialized proportional to the autoconversion rate given in the bulk microphysics scheme [*Seifert and Beheng*, 2001] for each grid box and each time step such that the mass of cloud water that is converted to rainwater in the bulk microphysics scheme equals the rainwater mass that is initialized with the LDs. We use a fixed initial multiplicity, ξ_0, and the initial position of an LD is chosen randomly within the grid box it is assigned to.

The distribution of the initial mass of raindrops in general depends on the pairs of cloud droplets that coalesce and form a raindrop as well as on the relative importance of condensation for the largest cloud droplets. This distribution could be analyzed with the superdroplet method or a spectral bin model but so far has not been investigated to the authors' knowledge. The initial mass of a raindrop is restricted between m^* and $2m^*$ where $m^* = 2.6 \times 10^{-10}$ kg is the minimal mass of a raindrop, which corresponds to a drop radius of 40 μm. In the bulk microphysics scheme of *Seifert and Beheng* [2001], 40 μm is chosen to be the drop radius that separates cloud droplets from raindrops. We decide to use a simple initial mass distribution, and choose a uniform distribution between m^* and $2m^*$. The actual initial mass of one of the raindrops represented by an LD, m_0, is then drawn randomly from this distribution. Using a uniform distribution presumably overestimates the mean initial size of the raindrops and hence underestimates the number of raindrops, which might lead to a slightly too early emergence of large raindrops for the LD model. Two sensitivity runs are performed: one with an initial LD mass distribution that decreases linearly to zero between m^* and $2m^*$ (sensitivity run 4 in Table 2) and one with all LDs initialized with m^* (sensitivity run 5). The development of the LD statistics is not very sensitive to the assumed initial mass distribution as long as it is allowed for some variability in the initial mass.

The average number of newly initialized LDs in a grid box is $N = A \Delta V \Delta t / M$, where A is the autoconversion rate, ΔV is the gridbox volume, Δt is the model time step, and M is the average total initial mass that an LD represents. For the control run, in which a uniform distribution of the initial mass is assumed, $M = 1.5 m^* \xi_0 = 195$ g. Because usually N is not a natural number, the actual number of newly initialized LDs is the largest natural number that is smaller than N, and a Monte-Carlo process is used to determine whether an additional LD is initialized that represents the decimal places of N. For instance, if $N = 5.3$, either 5 or 6 LDs are initialized and the probability that 5 LDs are initialized is 70%.

Finally, an LD is deactivated as soon as its mass shrinks below m^* or it reaches the ground. The sensitivity for using a smaller minimum mass is small (sensitivity run 6 in Table 2).

3.2. Trajectory

The momentum equation of an LD in a gravity field is obtained from the balance of the drag force, $F_d = 1/2 C_d \rho_a \pi r_{max}^2 |\vec{v}_a - \vec{v}_d|(\vec{v}_a - \vec{v}_d)$, the gravity force, $F_g = 4/3 \pi r^3 g(\rho_w - \rho_a)$, and the inertial force, $F_i = 4/3 \pi r^3 \rho_w d\vec{v}_d / dt$, giving

$$\frac{d\vec{v}_d}{dt} = \frac{1}{\tau_d}(\vec{v}_a - \vec{v}_d) - \left(1 - \frac{\rho_a}{\rho_w}\right) g \vec{e}_3 \tag{1}$$

$$\text{with} \quad \tau_d = \frac{8\rho_w r^3}{3\rho_a C_d r_{max}^2} \frac{1}{|\vec{v}_a - \vec{v}_d|} \tag{2}$$

Here $\vec{v}$ is the velocity vector of an LD and its ambient air indicated by the indices d and a, respectively. Then r is the LD's mass equivalent radius, i.e., the radius of the mass equivalent perfect sphere. To account for the flattening of large raindrops that deviate from a perfect sphere, we use the approximation from

Seifert et al. [2014] to specify the maximum dimension of the drop, r_{max}. The droplet relaxation time, τ_d, depends on the drag coefficient, C_d, which in turn is a function of the Reynolds number, $N_{Re} = 2r_{max}|\vec{v}_a - \vec{v}_d|/\nu$, i.e., depends on the drop's relative speed compared to its environmental air and on the size of the drop. The kinetic viscosity of air, ν, depends on temperature and is given by Sutherland's law [*Sutherland*, 1893]. Furthermore, $\vec{e}_3$ is the unit vector in vertical direction, g gravity, ρ_w the density of water, and ρ_a the density of air.

In equilibrium, the LD velocity is $\vec{v}_{d,\infty} = \vec{v}_a - v_t\vec{e}_3$ with v_t being the (equilibrium) terminal fall velocity of the drop relative to the moving fluid,

$$v_t = \tau_{d,\infty}\left(1 - \frac{\rho_a}{\rho_w}\right)g \tag{3}$$

Note that $\tau_{d,\infty}$ itself is a function of $\vec{v}_{d,\infty}$ and $\vec{v}_a$ (equation (2)). Inertial effects can be quantified by analyzing the deviation of the instantaneous LD velocity, $\vec{v}_d$, from its equilibrium value, $\vec{v}_{d,\infty}$. Accordingly, we also define an instantaneous fall velocity, $v_f = w_a - w_d$, which may differ from the terminal fall velocity, v_t. Here w is the vertical component of the velocity vector.

Because τ_d is small—mostly much smaller than the model time step, Δt—and slowly varying in time, equation (1) reveals properties of a stiff system and a third-order Runge-Kutta scheme is not appropriate to solve numerically for $\vec{v}_d$. To ensure that, independent of the time step of the LES model, the momentum equation of the LD is solved robustly, i.e., without spurious oscillations in the LD velocity, we use a procedure related to the idea of an exponential integrator [*Certaine*, 1960]. To predict the LD velocity, we first determine τ_d with a predictor-corrector method and then use the analytical solution of the momentum equation (equation (1)) to predict $\vec{v}_d$. The momentum equation can be solved analytically assuming that τ_d and $\vec{v}_a$ are constant for one time step and with the initial condition of $\vec{v}_d(t=0) = \vec{v}_{d,0}$ by

$$\vec{v}_d(t) = \left(\vec{v}_{d,0} - \vec{v}_a + \tau_d\left(1 - \frac{\rho_a}{\rho_w}\right)g\vec{e}_3\right)\exp\left(-\frac{t}{\tau_d}\right) + \vec{v}_a - \tau_d\left(1 - \frac{\rho_a}{\rho_w}\right)g\vec{e}_3 \tag{4}$$

For consistency with the Eulerian model, we update the LD position with a third-order Runge-Kutta scheme that considers the variability of $\vec{v}_a$.

Such a mixed approach of an analytical solution for the LD velocity with a predictor-corrector procedure for τ_d, and a third-order Runge-Kutta scheme for the LD position is equal to the analytical solution with the predictor-corrector method if $\vec{v}_a$ is constant during each time step. Asymptotically, if the mass of the drop vanished, τ_d and v_t approach zero and $\vec{v}_d$ is equal to $\vec{v}_a$, i.e., the result is equal to the third-order Runge-Kutta scheme for a massless particle.

Following *Abraham* [1970], a good approximation of C_d is given by

$$C_d = C_0\left(1 + \frac{\delta_0}{\sqrt{N_{Re}}}\right)^2 \tag{5}$$

with $C_0 = 0.29$ and $\delta_0 = 9.06$. For small N_{Re}, it follows that $C_d = C_0\delta_0^2/N_{Re} = 24/N_{Re}$, which matches the solution for the Stokes regime. For large raindrops, the flattened shape of the raindrop deviating from a perfect sphere and a turbulence correction of C_d should be considered [e.g., *Khvorostyanov and Curry*, 2002, 2005]. For $r = 500$ μm, the difference between the terminal fall velocity according to equations (3) and (5), and the terminal fall velocity from *Khvorostyanov and Curry* [2005] is 9 cm/s, i.e., less than 3% (Figure 1). Compared to the semiempirical formulas from *Beard* [1976], the difference is 24 cm/s for $r = 500$ μm, i.e., less than 7%. Because in this study the raindrops are mostly smaller, we neglect such corrections on $\vec{v}_t$ and use C_d as written in equation (5). Therefore, C_d is used consistently with equations (1) and (2) and also takes into account deviation from its equilibrium value, which can be caused by the LD velocity deviating from its terminal fall velocity due to inertial effects.

The fluid velocity that an LD feels is composed of two parts, the resolved fluid velocity of the ambient air and the subgrid-scale contribution: $\vec{v}_a = \vec{v}_{res} + \vec{v}_{sgs}$. The subgrid-scale velocity is calculated once every time step according to the approach from *Weil et al.* [2004], which has been developed for stationary, homogeneous, and isotropic turbulence, and noninteracting particles. Weil's prognostic equation for a Gaussian random subgrid-scale velocity forcing is based on the unresolved turbulent kinetic energy, which in turn is calculated by the Smagorinsky-Lilly model in UCLA-LES.
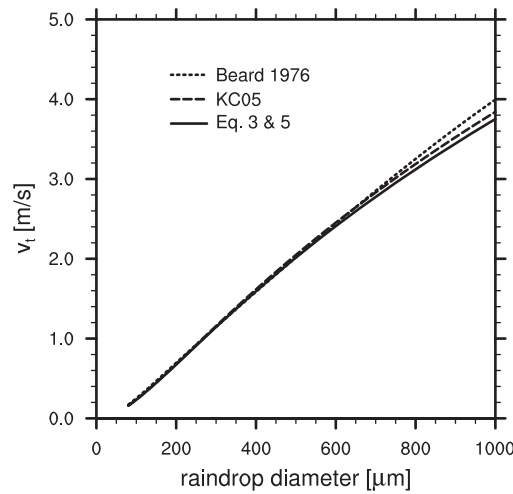
Figure 1. Terminal fall velocity for surface conditions of a standard atmosphere according to equations (3) and (5), and after *Khvorostyanov and Curry* [2005, KC05] and *Beard* [1976].

The Lagrangian subgrid-scale model from *Weil et al.* [2004] has been applied to massless, noninteracting Lagrangian particles in LES, e.g., to study mixing and entrainment in the convective boundary layer [*Heus et al.*, 2008; *Yamaguchi and Randall*, 2012]. However, the model has limitation when being applied to interacting Lagrangian drops. For a pair of particles, Weil's assumption of a random, uncorrelated subgrid-scale contribution to each particle's velocity becomes invalid if small separation distances between particles are considered, e.g., for point sources [*Bec et al.*, 2010]. In contrast, an identical subgrid-scale contribution for particle pairs with a negligible separation distance would neglect inertial effects. Using the concept of multiplicity, the actual LD concentration is lower than the raindrop concentration in a cloud. If the multiplicity was drastically reduced, i.e., the LD concentration increased, neglecting the subgrid-scale velocity correlation of particle pairs possibly alters the convergence behavior of the LD model.

For the control run, we include the subgrid-scale contribution according to *Weil et al.* [2004]. In addition, we perform a sensitivity run in which the subgrid-scale contribution to the LD's momentum equation is neglected and we discuss the effect of an uncorrelated subgrid-scale velocity on the collision rate in section 4.

3.3. Evaporation and Accretion

For the calculation of evaporation, we follow *Mason* [1971, p. 123] and additionally include the effect of ventilation:

$$\frac{\mathrm{d}m}{\mathrm{d}t}\bigg|_{\mathrm{evap}} = f_v 4\pi r \rho_w \frac{(S-1)}{(F_h+F_v)} \tag{6}$$

where $S-1$ is supersaturation, F_h describes conduction of heat, and F_v describes diffusion of water vapor. The factor f_v represents the effect of ventilation according to *Beard and Pruppacher* [1971] and *Pruppacher and Rasmussen* [1979], and depends on N_{Re} and on the Schmidt number for water vapor, $N_{\mathrm{Sc}} = v/D_v$, with $D_v = 2.5 \times 10^{-5}$ m²/s being the diffusivity of water vapor. In this approach, the effects of curvature and solution are neglected as well as kinematic and statistical, nonstationary growth effects, which is a reasonable assumption for raindrops of the sizes considered [e.g., *Rogers and Yau*, 1989, pp. 103 and 112]. For raindrops, the growth rate due to condensation is typically much smaller than the growth rate due to accretion and is not taken into account here.

For accretion, a continuous model of collection growth is used [*Pruppacher and Klett*, 1997, p. 617]. For the model to be valid, it is assumed that the collected cloud droplets are much smaller than the collector raindrop, i.e., that the cloud droplet fall velocity is much smaller than the raindrop fall velocity, and that the raindrop number density (typically <1 cm^{-3}) is much smaller than cloud droplet density (typically 100 cm^{-3}). Then the mass gain due to accretion is given by:

$$\frac{\mathrm{d}m}{\mathrm{d}t}\bigg|_{\mathrm{accr}} = E_c \pi \rho_a r_{\mathrm{max}}^2 |\vec{v}_d - \vec{v}_a| q_c \tag{7}$$

where m is the raindrop mass, q_c is the ambient cloud water mixing ratio, and the collision-coalescence efficiency, E_c, is set to unity. For maritime clouds with relatively large cloud droplets, $E_c = 1$ is justified but a parameterization of E_c as a function of the cloud droplet size distribution should to be considered if the typical cloud droplet size is smaller.

3.4. Selfcollection

Selfcollection of raindrops is important if the raindrop number density is high. Using a bulk microphysics scheme, *Stevens and Seifert* [2008] found that also for lightly precipitating shallow cumulus clouds,

selfcollection has an important effect on the precipitation amount. For a raindrop distribution, selfcollection overall reduces the number of raindrops but conserves the rainwater mass. Hence for the LD model, selfcollection redistributes mass among the LDs and reduces their multiplicity. The formulation of selfcollection for the LD model consists of two steps: first it is defined how a pair of LDs coalesces and second the probability of selfcollection is determined depending on this definition.

Concerning the first step of how LDs coalesce, we closely follow the approach of *Shima et al.* [2009]. For the selfcollection of a pair of LDs (j, k), the LD with the lower multiplicity retains its multiplicity while gaining mass and the LD with the higher multiplicity retains its mass while its multiplicity is lowered. For multiplicities ξ_j and ξ_k, where $\xi_j \neq \xi_k$ and without loss of generality $\xi_j < \xi_k$, the properties of the LDs after a selfcollection event (dashed variables) are

$$\xi'_j = \xi_j, \quad \xi'_k = \xi_k - \xi_j \tag{8}$$

$$m'_j = m_j + m_k, \quad m'_k = m_k \tag{9}$$

For $\xi_j = \xi_k$,

$$\xi'_j = \mathrm{floor}(\xi_j/2), \quad \xi'_k = \xi_k - \mathrm{floor}(\xi_j/2) \tag{10}$$

$$m'_j = m_j + m_k, \quad m'_k = m_j + m_k \tag{11}$$

For the second step, to determine the probability of selfcollection of a pair of LDs, we follow the approach of *Sölch and Kärcher* [2010] who suggest an algorithm for selfcollection that takes into account the vertical position of the LDs. Only if the difference between the vertical velocities of the LDs times the time step is larger than vertical distance between the LDs, selfcollection may take place. We consider all LD pairs within one grid column, i.e., we consider LDs falling across vertical grid box boundaries, but not across horizontal grid box boundaries. Collisions of a pair of LDs may occur within one model time step, Δt, if

$$0 < \frac{z_j - z_k}{w_{d,k} - w_{d,j}} \leq \Delta t \tag{12}$$

where z is the vertical position of the LD and w_d its vertical velocity. If this criteria is met and if a homogeneous distribution of raindrops in the horizontal of one grid box column is assumed, the probability for selfcollection for each pair of LDs (j, k), P_{jk}, is given by

$$P_{jk}^{\mathrm{CTRL}} = \frac{max(\xi_j, \xi_k)}{\Delta x \Delta y} E_c \pi (r_j + r_k)^2 \frac{|\vec{v}_{d,j} - \vec{v}_{d,k}|}{|w_{d,j} - w_{d,k}|} \tag{13}$$

where Δx and Δy are the horizontal dimensions of a grid box and $\pi(\Delta r)^2 |\Delta\vec{v}_d|/|w_d|$ is the projected sweep area of the raindrops. The last factor of equation (13), $|\Delta\vec{v}_d|/|\Delta w_d|$, approaches one if the vertical component of the LD velocities dominates the velocity difference of a pair of LDs. We use this formulation of LD selfcollection given in equations (8)–(13) for the control run.

Alternatively, it may also be assumed that the raindrops an LD is representing are distributed homogeneously within one grid box not only in the horizontal but also in the vertical. This follows the ideas of *Shima et al.* [2009, hereinafter S09] except for their Monte-Carlo sampling of superdroplet pairs that we do not apply. Then the probability of selfcollection for each pair of LDs (j, k) that is located in the same grid box is

$$P_{jk}^{\mathrm{S09}} = E_c \frac{max(\xi_j, \xi_k)}{\Delta x \Delta y \Delta z} \pi (r_j + r_k)^2 \Delta t |\vec{v}_{d,j} - \vec{v}_{d,k}| \tag{14}$$

where Δz is the vertical size of a grid box and $\pi(\Delta r)^2 \Delta t |\Delta\vec{v}_d|$ is the sweep volume of the raindrops. Again, in case that the vertical velocity difference dominates the velocity difference of a pair of LDs, the last factor, $|\Delta\vec{v}|$, could be replaced by the vertical velocity difference, $|\Delta w|$. The assumption of homogeneously distributed raindrops within each grid box, may overestimate the probability for selfcollection, if due to gravitational sorting and raindrop growth heavier (i.e., larger) drops tend to be positioned lower within a grid box. If heavier drops are positioned lower in a grid box, they are not able to capture the smaller drop above them according to P_{jk}^{CTRL} (equation (13)) but are considered in P_{jk}^{S09} (equation (14)). We will show later in

section 4, that the horizontal velocity difference of a pair of LDs contributes noticeably to their total velocity difference and that the effect of gravitational sorting in a grid box on the selfcollection can indeed be neglected in the cases considered.

For both approaches, P_{jk}^{CTRL} and P_{jk}^{S09} equal the expected value of the selfcollections of $min(\xi_j, \xi_k)$ pairs of real drops. However, due to the rather small number of LDs (compared to the number of raindrops in a real cloud), the variance of the number of coalesced pairs is overestimated by the LD model (for a detailed discussion of the expectation value and variance, see *Shima et al.* [2009]).

For selfcollection, it is not justified to set the collision-coalescence efficiency, E_c, to unity. Instead, the coalescence efficiency depends on the raindrop size and is determined following the measurements of *Beard and Ochs* [1995]. Using such a parameterization for E_c can also be understood as an attempt to take raindrop breakup into account, i.e., be interpreted as a pair of raindrops rebouncing from each other without changing their masses. For raindrops larger than those considered here, filament breakup becomes an important process [*Low and List*, 1982; *Seifert et al.*, 2005; *Straub et al.*, 2010] but is not taken into account in this study.

We use a Monte-Carlo sampling to determine whether two LDs, that have the probability P_{jk} to collide, do collide in the model.

The position and the velocity of the LDs are assumed to remain unchanged directly after selfcollection.

3.5. Implementation
The LDs are implemented as a linked list of particles with several properties. For each processor, a maximum length of the list is specified a priori and represents a "reservoir" of LDs. From that reservoir particles are activated as LDs according to the autoconversion rate on that part of the grid that the particular processor represents. When LDs leave the spatial domain of the processor, they are passed to the linked list of the processor they enter. Once an LD is deactivated, because it shrinks below a threshold or reaches the surface, it is passed back to the linked list of its home processor. There, it is available for activation again. To distinguish the former LD (and its trajectory) from the newly activated one, each LD has a property called *drop number*, which is increased by a value of one if a new LD is activated. To find potential pairs of LDs for selfcollection more effectively, the LDs are also sorted and linked on an additional three-dimensional variable spanning the spatial grid.

The fixed reservoir size per processor, which is specified before starting the model, has only become necessary due to limitations in the output to NetCDF. Before particle output is written, all particles are passed back to their home processor so that the number and order of particles for each output time step is fixed. Using such a static array for writing data ensures an efficient output routine while the usage of a linked list in principle allows for a dynamic internal memory management. Particle properties are written to disk every 15 s of simulation time to be able to analyze an LD's trajectory and growth history. For each particle, 22 variables are saved. Ten of them give properties of the LD: the drop number, the mass and multiplicity, the relaxation time scale, the three components of the LD position in space, and the three velocity components of the instantaneous LD velocity. In addition, 12 properties of the flow at the LDs position are saved: the three components of the fluid velocity and the three components of the subgrid-scale contribution to the fluid velocity, the potential temperature, the virtual potential temperature, the cloud liquid water, the total water, the dissipation rate, and the pressure.

The computational overhead of the LD model depends on the number of particles per reservoir and on the number of active LDs. The runs analyzed in this study are all run on 32 processors and most of them use a reservoir which corresponds to two particles per grid box, i.e., depending on the domain size there are about 1.5×10^5 particles available per processor or roughly 5×10^6 particles for the whole domain. For the sensitivity run with quartered initial multiplicity, the number of particles is doubled, i.e., there are four particles in the reservoir per grid box. Without the LD model, one LES run needs about 1800 CPU h, for the runs with the LD model and two LDs per grid box about 3400–3800 CPU h are consumed and for four LDs per grid box 4800 CPU h are needed. Therefore, the computational overhead due to the LD model is typically about 100% for the runs performed for this study. Nevertheless, the limiting factor for these simulations is mostly the available disk space for the output of all LDs, not the actual CPU time consumed for the run.

4. Resolved and Subgrid-Scale Turbulent Velocity Fluctuations and Their Effect on Collision Frequency

While sensitivities to some assumptions of the LD model such as the initial multiplicity, the initial mass distribution, or the minimum mass are rather small for a reasonable range of parameters (sensitivity runs 1–6 in Table 2), we find that the LD model shows a more pronounced sensitivity to the treatment of selfcollection. Besides the radius and the multiplicity, the selfcollection rate depends on the velocity difference between a pair of LDs (section 3.4). Therefore, we first discuss the impact of inertial effects on the LD's velocity, and then expand the discussion on effects that impact the collision probability such as the subgrid-scale velocity.

To analyze the effect of inertia on the instantaneous vertical drop velocity, we define the normalized vertical velocity deviation of an LD, $\Delta w/v_t = (w_d - w_a + v_t)/v_t$, which characterizes the strength of inertial effects on the raindrop velocity and is zero if inertial effects are negligible, i.e., if the instantaneous fall velocity is equal to the fluid velocity minus the terminal fall velocity. For the control run, the normalized vertical velocity deviation is rarely as large as 20% and is less than 5% more than 90% of the time (Figure 2). Neglecting the subgrid-scale contribution of the fluid velocity on the LD's momentum equation narrows the distribution of the normalized vertical velocity deviation of an LD even further.

Observations of more heavily precipitating cases have found that "superterminal" raindrops, i.e., raindrops that fall faster than their terminal fall velocity ($\Delta w/v_t < 0$), are abundant for raindrop diameters <1 mm [*Montero-Martínez et al.*, 2009; *Larsen et al.*, 2014]. *Montero-Martínez et al.* [2009] suggest that those superterminal raindrops are caused by the breakup of very large raindrops, whose fragments directly after the breakup event still fall with the higher fall velocity of the original raindrop and then slow down with time by relaxing to their own terminal fall velocity. To be able to investigate the occurrence of such a mechanism with the LD model, a detailed formulation for breakup of large raindrops still has to be included in the LD model. From our current simulations, we find no evidence for a large fraction of superterminal raindrops.

The rather small effect of inertia on the LD's velocity observed in this study is consistent with the values of the Stokes number of the LDs, $St = \tau_d/\tau_\eta$, where $\tau_\eta = \sqrt{\nu/\epsilon}$ is the Kolmogorov time scale and ϵ the dissipation rate (calculated as described in *Stevens et al.* [1999]). For large Stokes numbers, the LD relaxation time scale, τ_d, is larger than the Kolmogorov time scale, τ_η, and inertial effects are important. The Stokes number is >1 for 18% of the LDs in cloud A and for only 6% of the LDs in cloud B (Figure 3). Stokes numbers >5 are very rare (0.28% for cloud A and 0.01% for cloud B). Although the relaxation time scale is increasing almost linearly with the LD diameter for the range considered, the spread in Stokes numbers is large because LDs of different size do not sample the three-dimensional domain homogeneously. Small LDs dominate regions with high dissipation rates near cloud top where the autoconversion rate is high. In contrast, large LDs are often located in less turbulent regions with low dissipation rates both inside the cloud and outside the cloud in the environmental air.

To investigate the effects of velocity deviations due to inertial effects in the LD's momentum equation (equation (4)) on the development of the RSD, we perform a sensitivity run where instead of applying a relaxation time scale, τ_d, the LD's velocity is simply set to $\vec{v}_d = \vec{v}_a - v_t \vec{e}_3$, i.e., explicit inertial effects are neglected in the momentum equation ("traj.: no inertia" in Figure 4, sensitivity run 12 in Table 2). Because the fluid velocity, $\vec{v}_a$, is the sum of the resolved fluid velocity and a contribution from the Lagrangian subgrid-scale model, this setup still allows for velocity differences between a pair of LDs at the same location due to the subgrid-scale contribution. Compared to the control run, the RSD and the surface precipitation rate do not differ noticeably. This implies that the effect of the vertical velocity deviations as shown in Figure 2 (i.e., the difference between the control run and a delta function at zero) and of the corresponding horizontal velocity deviations on the LD growth is small.

The horizontal velocity difference of two LDs that are located close to each other is increasing with increasing separation distance (Figure 5). This has implication for the representation of selfcollection in the LD model: using the concept of multiplicity, collision probabilities in the LD model are calculated for all LD pairs that are located within the same grid box (equation (14); or within the same column and within a vertical distance that is defined by their vertical velocity difference, equations (12) and (13)). Real raindrops,

(a) cloud A (b) cloud B
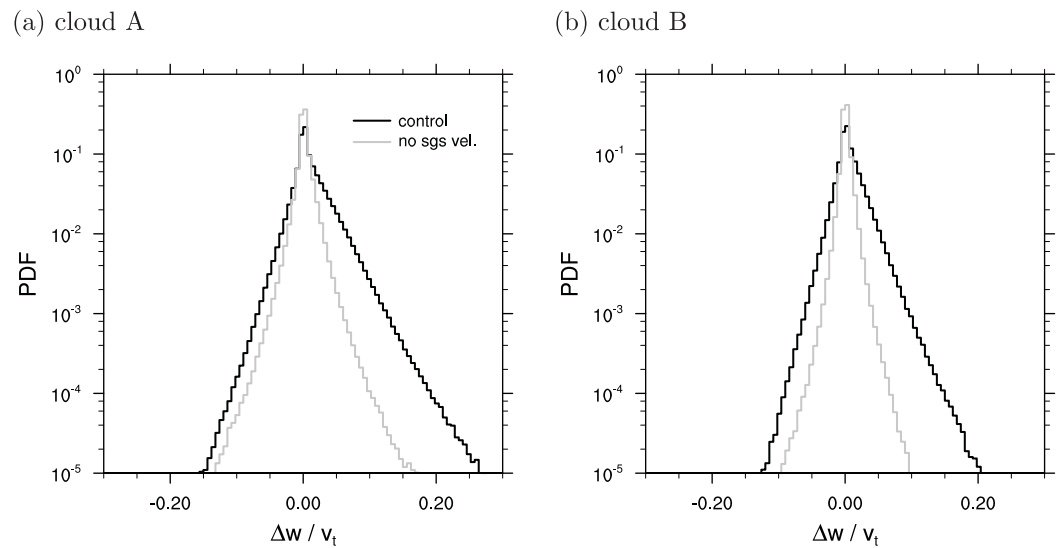
Figure 2. Normalized vertical velocity deviation, $\Delta w/v_t = (w_d - w_a + v_t)/v_t$. Values are positive if the LD is falling down slower than its equilibrium terminal fall velocity would suggest; for negative values, the LD is falling faster.

however, only collide if they meet at the same position. Because collisions are considered for LD pairs within a grid box regardless of their separation distance, the horizontal velocity difference of a pair of LDs is overestimated for the collision rate in the LD model. However, due to inertial effects we do not expect the horizontal velocity difference to be zero either.

A second issue concerning the velocity difference of a pair of LDs for the collision rate arises from the use of a Lagrangian subgrid-scale model. The subgrid-scale contribution to the fluid velocity directly influences the LD's trajectory via its momentum equation but also impacts the relative velocity difference between a pair of LDs and therefore the collision rate (equations (13) and (14)). Switching off the subgrid-scale contribution for a sensitivity run ("traj.: no sgs vel.," Figures 5c and 5d), the average horizontal velocity difference of a pair of LDs is smaller than for the control run that includes the subgrid-scale contribution (Figures 5a and 5b). Including the subgrid-scale contribution, we find that the horizontal velocity difference is higher especially for those pairs of LDs that are located close to each other. Here the horizontal velocity difference

(a) cloud A (b) cloud B
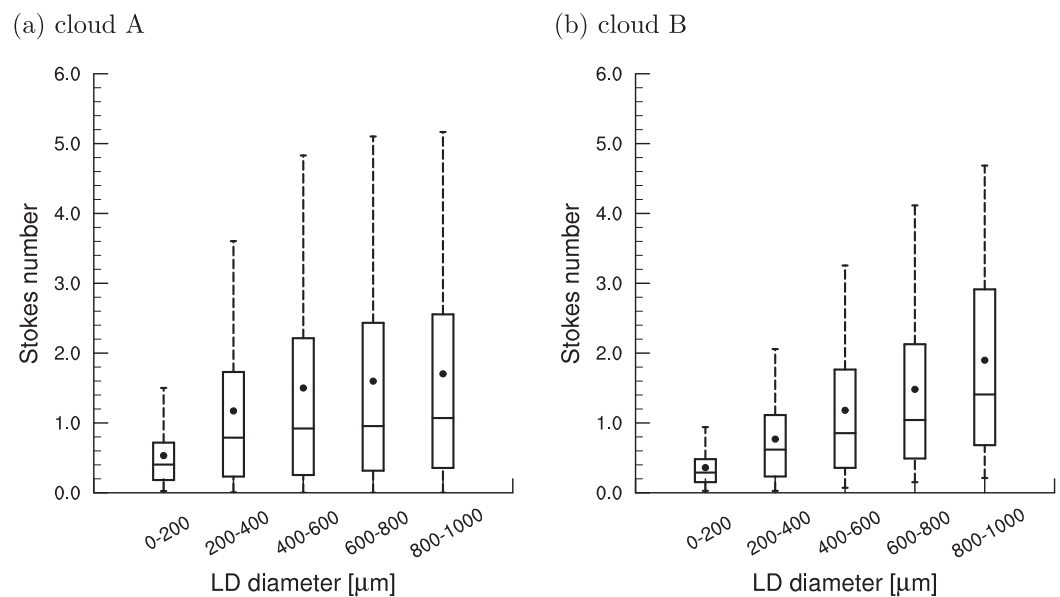
Figure 3. Boxplot of the Stokes number of the LDs as a function of the LD diameter. The whiskers and the boxes mark the 5%, 25%, 50%, 75%, and 95% percentiles, and the dots mark the mean.
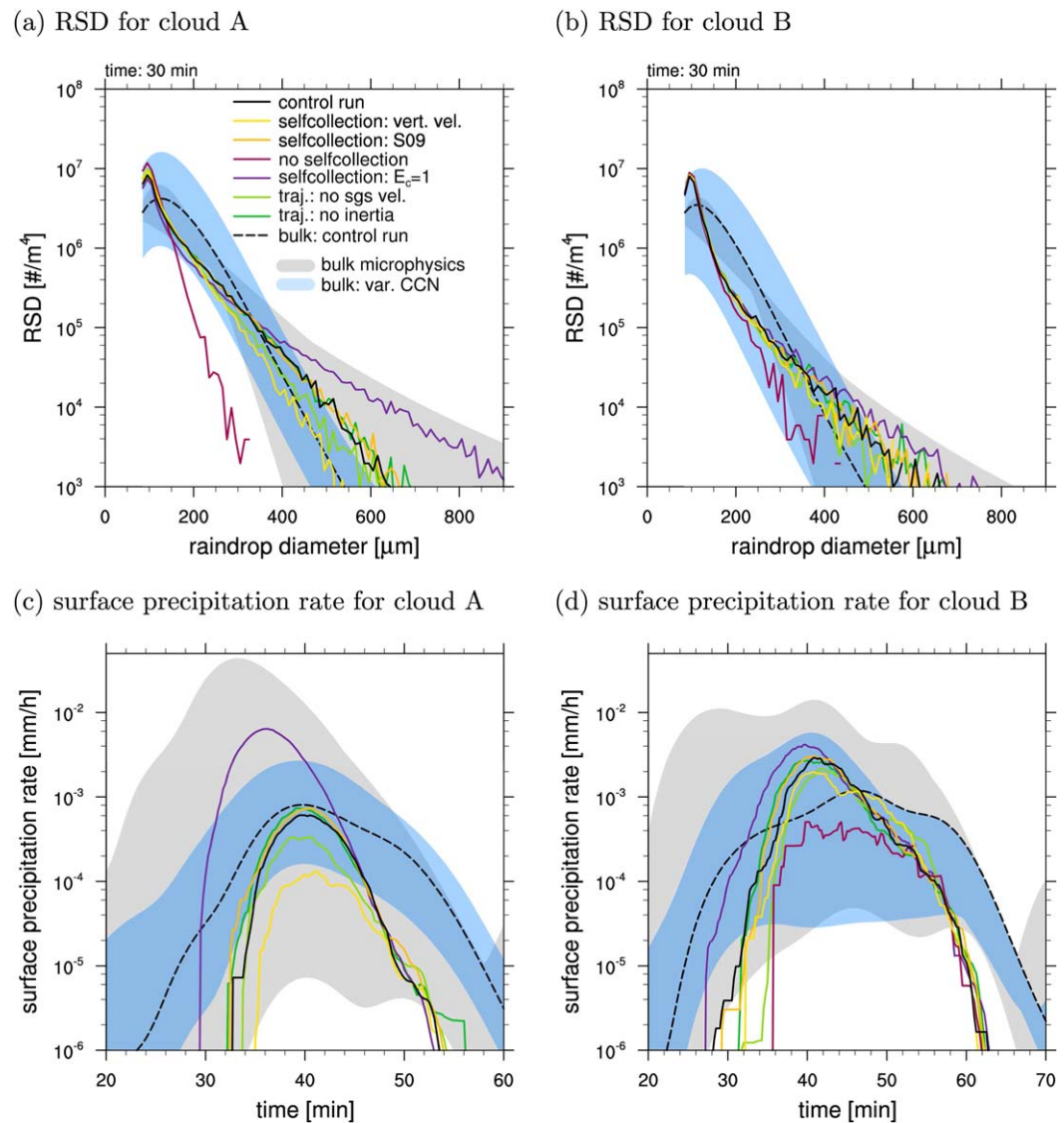
Figure 4. Raindrop size distribution (RSD) and 2 min running average of the surface precipitation rate for the control run and selected sensitivity runs. The grey area indicates the uncertainties in the bulk rain microphysics scheme due to the choice of the shape parameter of the RSD (see section 5 for explanation). The blue area gives the sensitivity of the bulk scheme to decreasing and increasing the cloud droplet density by 50%.

is probably overestimated by the subgrid-scale model from *Weil et al.* [2004] because the subgrid-scale model neglects velocity correlations among LD pairs (see section 3.2) [*Yang et al.*, 2008; *Wang et al.*, 2009].

Recent superdroplet studies treat both issues differently. They either neglect the subgrid-scale contribution on the collision rate [*Shima et al.*, 2009; *Andrejczuk et al.*, 2010] or include it in an average sense by using a mean field approach derived from direct numerical simulations rather than a statistical approach for collision-coalescence [*Riechelmann et al.*, 2012]. All three studies assume collisions of superdroplets within a certain volume. In the collision kernel, *Shima et al.* [2009] include horizontal velocity differences of a pair of superdroplets and assume that the superdroplet's fall velocity equals its terminal fall velocity. *Andrejczuk et al.* [2010] consider only the vertical velocity difference of a pair of superdroplets.

To explore both the effect of the subgrid-scale contribution on the collision rate and the effect of the separation distance on the horizontal velocity difference (and thereby on the collision rate), we compare three simulations. In the control simulations, the Lagrangian subgrid-scale model with the uncorrelated velocity differences is used, and the horizontal velocity difference of a pair of LDs contributes to the collision probability. Two sensitivity runs are performed: in the first one, the subgrid-scale contribution to the LD velocity is

(a) control run for cloud A

(b) control run for cloud B

(c) traj.: no sgs vel. for cloud A

(d) traj.: no sgs vel. for cloud B
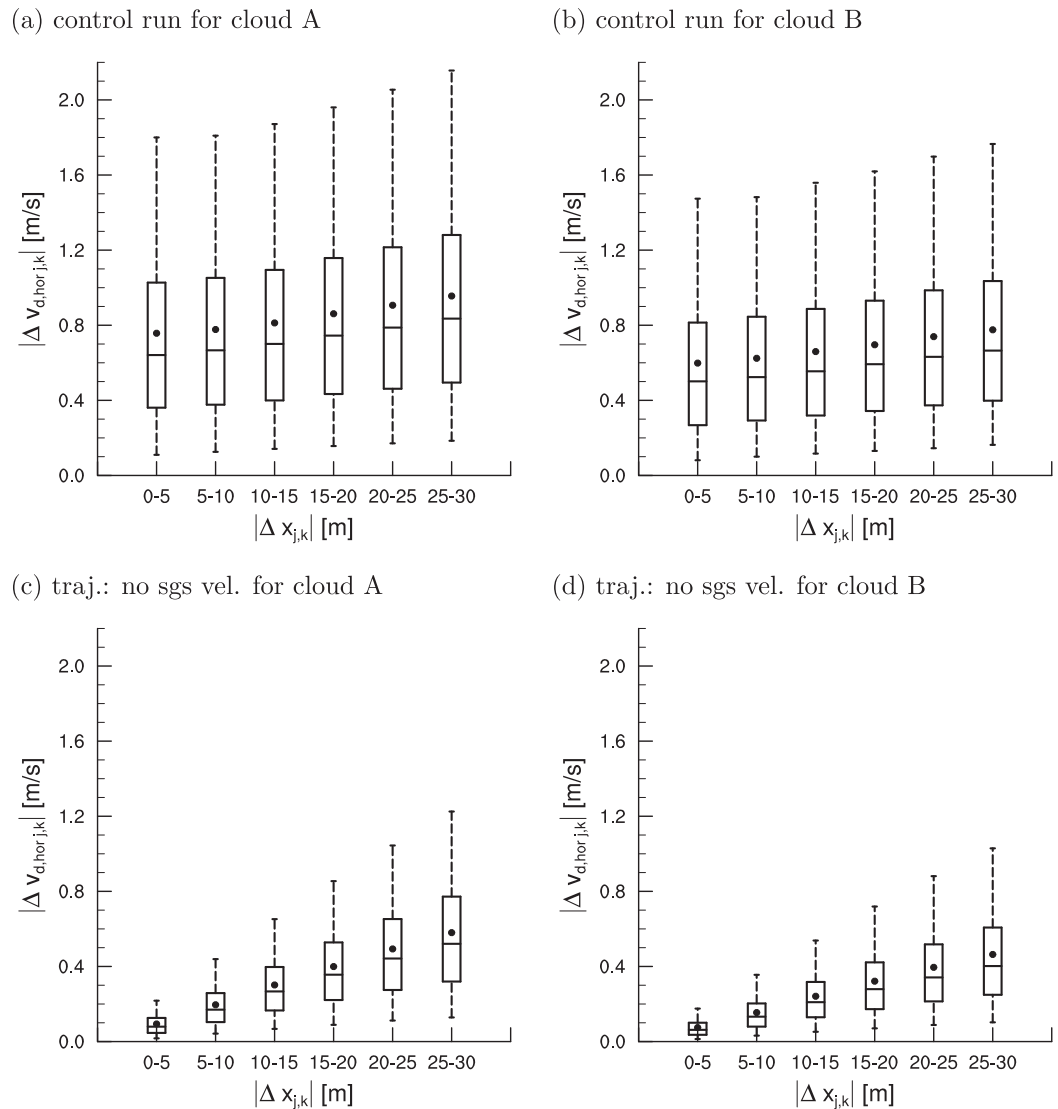
Figure 5. Boxplot for the horizontal velocity difference of pairs of LDs that are located in the same grid box as a function the LD separation distance. The whiskers and the boxes mark the 5%, 25%, 50%, 75%, and 95% percentiles, and the dots mark the mean.

neglected ("traj.: no sgs vel." in Figure 4, sensitivity run 11 in Table 2), which underestimates the collision rate in that respect. In the second one, the subgrid-scale model is applied, but only the vertical velocity difference of a pair of LDs is considered for the collision rate ("selfcollection: vert. vel.," sensitivity run 7). This also underestimates the collision rate because the contribution of the horizontal velocity difference is neglected. For both sensitivity runs, the surface precipitation is notably reduced for cloud A (to 55% and to 21%, respectively) and the RSDs are narrower compared to the control simulation.

To quantify these effects in the collision kernel, we analyze the vertical velocity difference of an LD pair normalized by the magnitude of its three-dimensional velocity vector (Figure 6). If the masses of an LD pair differ substantially, the velocity difference of a pair of LDs is dominated by the sedimentation velocity difference, i.e., the normalized vertical velocity difference is close to one. For small mass differences, the horizontal velocity difference may also contribute noticeably to the three-dimensional velocity difference and therefore the normalized vertical velocity difference is substantially lower.

For both the control run and the sensitivity run without the Lagrangian subgrid-scale model, the spread in normalized vertical velocity difference is high. For the control run, the average normalized vertical velocity difference is about 55%, i.e., using only the vertical velocity difference instead of the three-dimensional one,
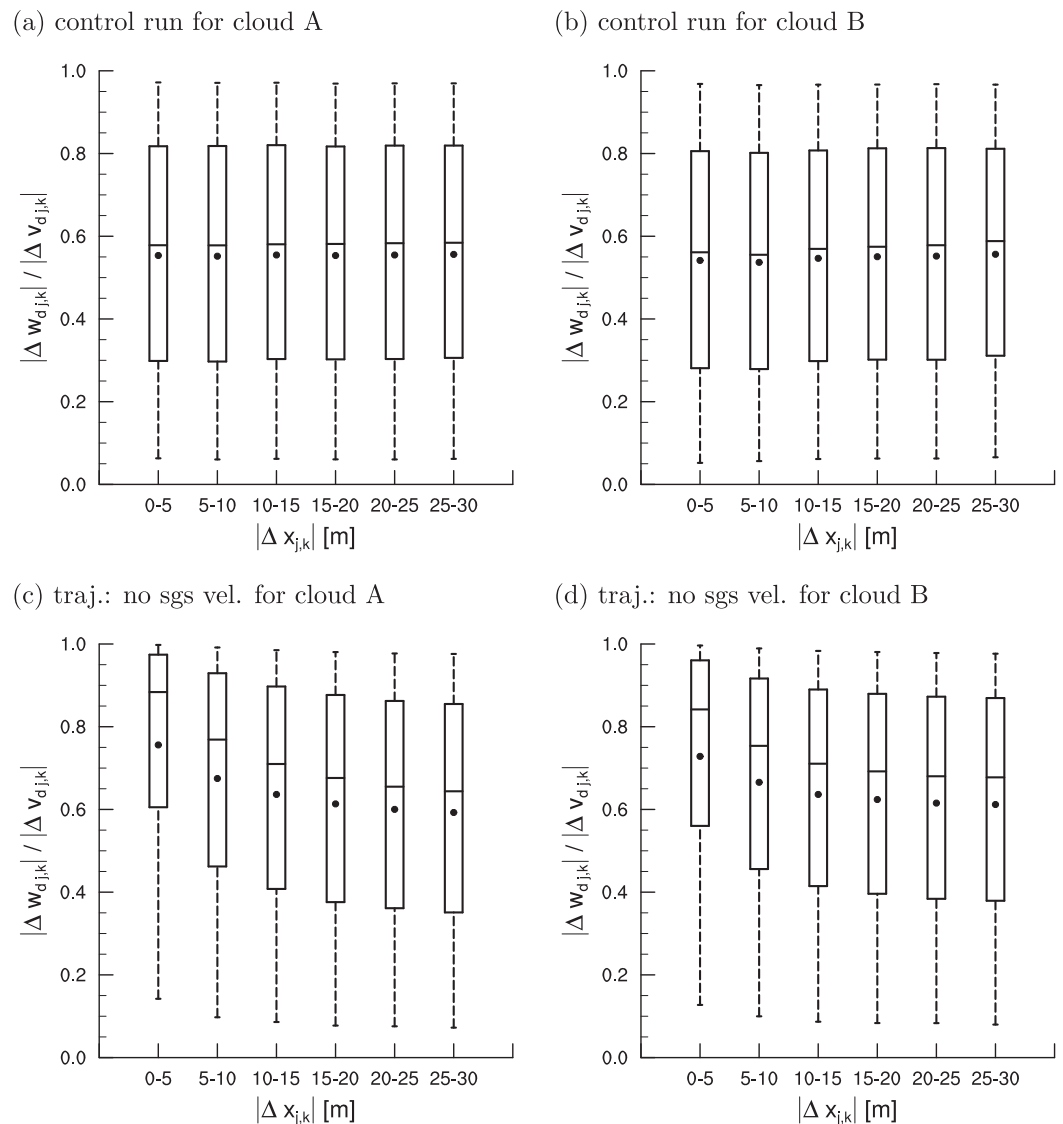
Figure 6. As Figure 5 but for the vertical velocity difference of LD pairs normalized by the magnitude of the three-dimensional velocity vector.

such as it is done in a classical gravitational kernel, on average reduces the collision rate by 45% compared to the control run. Without the Lagrangian subgrid-scale model, the average normalized vertical velocity difference is about 5% higher than for the control run and increases with decreasing separation distance.

This leads us to the conclusion that both the subgrid-scale contribution of the fluid velocity as well as the horizontal velocity difference, which is connected to the separation distance of a pair of LDs, do have a noticeable effect on the collision rate. All variants discussed here (the control run, the sensitivity runs "traj.: no sgs vel.," and "selfcollection: vert. vel.") have their issues and it is not obvious which implementation is most realistic leaving us with a considerable uncertainty in the formulation of the selfcollection of the LDs. Therefore, both effects should be explored further, e.g., by using a Lagrangian subgrid-scale model that includes correlation statistics for particles that are located close to each other [*Mazzitelli et al.*, 2014].

The assumption of a vertically homogeneous distribution of raindrops within one grid box [*Shima et al.*, 2009] instead of taking their vertical position into account [*Sölch and Kärcher*, 2010] does not have a distinct effect for cloud A or cloud B. Therefore, gravitational sorting within one grid box is not important for selfcollection in this case.

While all the sensitivity analyses above are physically reasonable and give an estimate of the uncertainty in the LD model, two further sensitivity runs make rather crude simplifications and again highlight the

importance of the selfcollection process: neglecting selfcollection altogether ("no selfcollection" in Figure 4, sensitivity run 9 in Table 2) results in a very narrow RSD and the absence of surface precipitation for cloud A. A constant collision-coalescence efficiency equal to unity ("selfcollection: $E_c = 1$," sensitivity run 10) results in a very broad RSD and a large increase in surface precipitation.

For cloud B, the tested sensitivities are consistent in sign with cloud A but overall lower in magnitude, both for the RSD and for the surface precipitation rate (Figure 4 and Table 2). Because cloud B has a more complex and overall longer lifecycle showing features of pulsating growth, we speculate that this less sensitive behavior is related to a microphysical buffering that compensates for changes, e.g., in selfcollection. Large normalized vertical velocity deviations and large Stokes numbers are even less numerous for cloud B than for cloud A due to an overall less vigorous lifecycle.

5. Assessment of the Bulk Microphysics Scheme

For both cloud A and cloud B, the LD statistics show some agreement with the bulk rain microphysics control run, which uses the closure equation of *Seifert* [2008] for the shape parameter of the RSD ("bulk: control run"
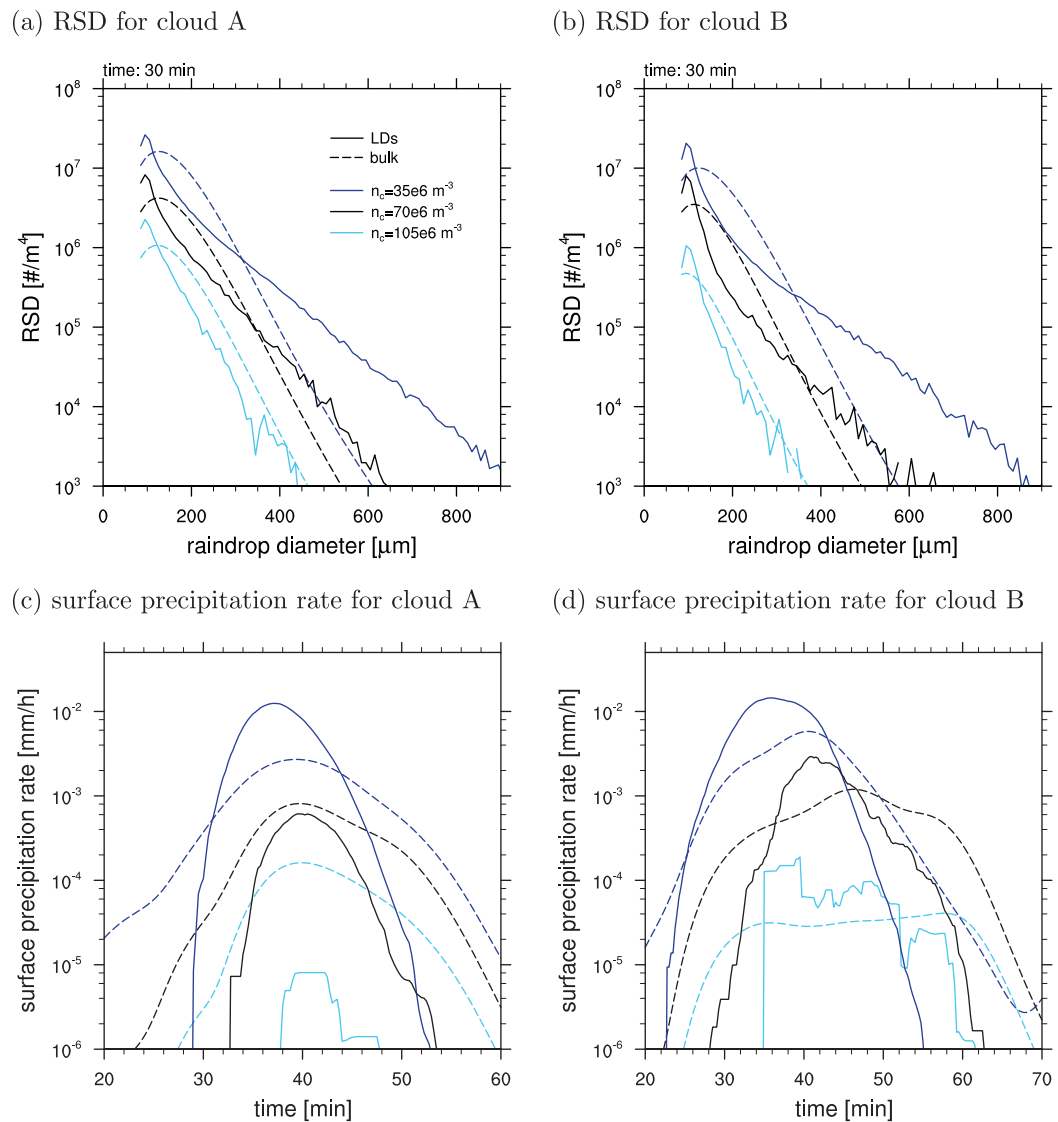
Figure 7. Raindrop size distribution (RSD) and 2 min running average surface precipitation rate for different assumptions of the cloud droplet number density, n_c.

in Figure 4 and Table 2). In the two-moment bulk microphysics scheme from *Seifert and Beheng* [2001], the RSD is assumed to follow a gamma distribution in terms of the raindrop diameter. Because the gamma distribution has three free parameters and only two of those can be determined from the prognostic moments of the parameterization, a closure equation for the third parameter, usually the shape parameter, is needed. To set the sensitivities of the LD model in context to the uncertainties in the bulk rain microphysics scheme, a set of four Eulerian simulations is run. Each simulation has been started from the same initial conditions and with the same Eulerian model setup as described in section 2.1 despite a change in the closure equation that determines the shape of the RSD in the bulk scheme. In addition to the control run, which uses the closure equation from *Seifert* [2008], three simulation are run: one using the closure equation suggested by *Milbrandt and Yau* [2005, MY05 in Table 2], one using a constant shape parameter equal to 1, and one using a constant shape parameter equal to 10. Considering the uncertain knowledge about the value of the shape parameter, besides the relations from *Seifert* [2008] and *Milbrandt and Yau* [2005] also a constant value of 1 and a constant value of 10 are plausible choices [*Stevens and Seifert*, 2008]. In Figure 4, the uncertainty in the RSD and the surface precipitation rate due to the choice of the shape parameter in the bulk scheme is given as a grey shading and only the control run is shown explicitly (dashed line). From Figure 4 and Table 2 (sensitivity run I–III), it can be seen that the uncertainty range of the bulk scheme due to the choices for the shape parameter of the assumed RSD is much larger than the uncertainty in the LD model.

An additional uncertainty of the bulk scheme lies in the treatment of the cloud droplet number density, n_c. In the bulk scheme, n_c is assumed to be constant in space and time, and aerosol effects are often studied by varying n_c [e.g., *Savic-Jovcic and Stevens*, 2008]. If n_c is decreased and to a first order it is assumed that the cloud water content is constant, the mean cloud droplet diameter and the autoconversion rate increase, i.e., more cloud water is converted to rainwater. In our control run, $n_c = 70 \times 10^6$ m^{-3} is prescribed in accordance with the RICO case setup [*van Zanten et al.*, 2011]. When decreasing n_c by 50%, the rainwater content is increasing (and vice versa for increasing n_c) but the slope of the RSD in the bulk scheme does not vary much (Figure 7 and sensitivity runs IV–V in Table 2). For the LD model, the tail of the RSD flattens with decreasing n_c (sensitivity run 13–14), i.e., with increasing rainwater content, the number of large raindrops increases disproportionally strong, probably due to more efficient selfcollection. Therefore, with decreasing n_c, the surface rain rate also increases more for the LD model than for the bulk scheme.

Overall, the uncertainty of the LD model, e.g., for the treatment of selfcollection, is smaller than the n_c sensitivity in both the bulk scheme and the LD model. The uncertainty of the bulk scheme due to the choice of the shape parameter of the RSD is at least as large as the impact of n_c.

6. Conclusions

We introduced a Lagrangian drop (LD) model to study warm rain microphysical processes. The LD model presented here is closely related to the superdroplet method and applies their concept of multiplicity but instead of trying to represent the whole drop size distribution it simulates the raindrop phase only, making the problem computationally more feasible. The LDs are initialized proportional to the autoconversion rate of the bulk microphysics scheme to assure that the same amount of rainwater is initialized in the bulk scheme and in the LD model. All relevant microphysical processes—accretion of bulk cloud water, selfcollection among the LDs, and evaporation in unsaturated air—are included so that the mass of an LD develops according to its environment. The momentum equation for each LD includes dynamical effects such as sedimentation and inertia, and a contribution from the parameterized subgrid-scale fluid velocity.

The LD model is intended to be used as a tool to understand warm rain microphysical processes in shallow cumulus on a particle-based level. In the present study, we test whether the model is fit for purpose. We therefore conduct a sensitivity study of two isolated shallow cumulus clouds that are simulated with Large-Eddy Simulations (LES) including a bulk microphysics parameterization and with the LD model for raindrop growth without feedbacks to the Eulerian LES fields. We show that the surface precipitation rate and the slope of the raindrop size distribution (RSD) are especially sensitive to the treatment of selfcollection in the LD model. Some uncertainty remains in determining the velocity difference of a pair of LDs, which appears as a factor in the collection kernel. On the one hand, a pure gravitational kernel underestimates the collection rate because it neglects the horizontal component of the velocity difference of a pair of LDs. On the other hand, a Lagrangian subgrid-scale model that does not take velocity correlations among particle pairs into account overestimates the

collision rate. In contrast, gravitational sorting within an LES grid box and other parameters such as the initial mass distribution or the initial multiplicity are found to have no distinct effect on the development of the RSD.

Comparing the LD model to the bulk microphysics scheme, we find that the tail of the RSD is less sensitive to changes in the cloud droplet number density for the bulk scheme than for the LD model. The uncertainties due to assumptions in the LD model—including those in the treatment of selfcollection—are much smaller than uncertainties of the bulk rain microphysics scheme due to assumptions on the shape parameter and the cloud droplet number density.

We therefore conclude that the LD model is a valuable tool for further studies to advance understanding of raindrop growth and dynamics. Possible applications to specific research questions include, e.g., the effect of evaporation on the RSD or the growth history of raindrops (see section 1). In a follow-up paper, we will use the LD model to investigate the importance of recirculation for rain formation in shallow cumuli.

Appendix A: Density Dependence of the Terminal Fall Velocity

The terminal fall velocity of a raindrop is not solely determined by its mass but also depends on the air density. For the LD model, this is taken into account via the temperature dependency of the air viscosity. (The pressure dependence is much smaller and thus neglected.) For a bulk rain microphysics scheme, the deceleration of a raindrop with increasing density, i.e., decreasing height, is usually considered by applying a density correction to the terminal fall velocity that is valid for sea level conditions, $v_{t,0}$. The terminal fall velocity at any height, v_t, is then given by *Beard* [1985]

$$\frac{v_t}{v_{t,0}} = \left(\frac{\rho_{a,0}}{\rho_a}\right)^m \tag{A1}$$

where $\rho_{a,0}$ is the air density at sea level, ρ_a is the actual air density, and m is the air density exponent. When taking the temperature dependence of the air viscosity into account [*Sutherland*, 1893], using the approach of *Abraham* [1970] to calculate the drag coefficient (equation (5)) and assuming a standard atmosphere to relate the air density and the temperature, m is increasing from about 0.2 for cloud droplets to 0.5 for large raindrops, i.e., small droplets decelerate less with decreasing height than large raindrops (Figure 8). Very similar values of m are obtained using the temperature and pressure correction from *Khvorostyanov and Curry* [2005]. In contrast, neglecting the temperature dependence of the air viscosity, results in increasing values of m with decreasing drop radius, i.e., an erroneous dependence of m on drop size. Because for large raindrops it is well established that m approaches 0.5, bulk rain microphysics schemes typically assume $m = 0.5$ when accounting for the density dependence of the terminal fall
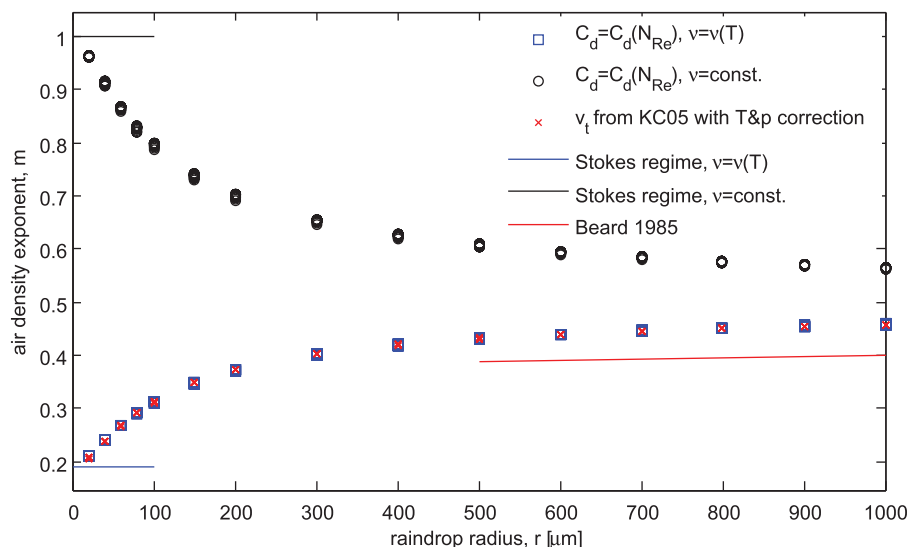
Figure 8. Air density exponent, m, as a function of the raindrop radius for different assumptions of the air viscosity.

velocities of raindrops. In this study, raindrops have a typical radius of 100–200 μm, and therefore, we choose to use a lower, more appropriate value of $m = 0.35$ in the bulk rain microphysics scheme (raindrop sedimentation and accretion).

References

Abraham, F. F. (1970), Functional dependence of drag coefficient of a sphere on Reynolds number, *Phys. Fluids*, *13*, 2194–2195.

Andrejczuk, M., J. M. Reisner, B. Henson, M. K. Dubey, and C. A. Jeffery (2008), The potential impacts of pollution on a nondrizzling stratus deck: Does aerosol number matter more than type?, *J. Geophys. Res.*, *113*, D19204, doi:10.1029/2007JD009445.

Andrejczuk, M., W. W. Grabowski, J. Reisner, and A. Gadian (2010), Cloud-aerosol interactions for boundary layer stratocumulus in the Lagrangian cloud model, *J. Geophys. Res.*, *115*, D22214, doi:10.1029/2010JD014248.

Beard, K. V. (1976), Terminal velocity and shape of cloud and precipitation drops aloft, *J. Atmos. Sci.*, *33*, 851–864.

Beard, K. V. (1985), Simple altitude adjustments to raindrop velocities for Doppler radar analysis, *J. Atmos. Oceanic Technol.*, *2*, 468–471.

Beard, K. V., and H. T. Ochs (1995), Collisions between small precipitation drops. Part II: Formulas for coalescence, temporary coalescence, and satellites, *J. Atmos. Sci.*, *52*, 3977–3996.

Beard, K. V., and H. R. Pruppacher (1971), A wind tunnel investigation of the rate of evaporation of small water drops falling at terminal velocity in air, *J. Atmos. Sci.*, *28*, 1455–1464.

Bec, J., L. Biferale, A. S. Lanotte, A. Scagliarini, and F. Toschi (2010), Turbulent dispersion of inertial particles, *J. Fluid Mech.*, *645*, 497–528.

Beheng, K. D. (1994), A parameterization of warm cloud microphysical conversion processes, *Atmos. Res.*, *33*, 193–206.

Certaine, J. (1960), The solution of ordinary differential equations with large time constants, in *Mathematical Methods for Digital Computers*, pp. 128–132, John Wiley, N. Y.

Grabowski, W. (2014), Extracting microphysical impacts in large-eddy simulations of shallow cumulus, *J. Atmos. Sci.*, *71*, 4493–4499.

Heus, T., and H. J. J. Jonker (2008), Subsiding shells around shallow cumulus clouds, *J. Atmos. Sci.*, *65*(3), 1003–1018, doi:10.1175/2007JAS2322.1.

Heus, T., G. van Dijk, H. J. J. Jonker, and H. E. A. V. den Akker (2008), Mixing in shallow cumulus clouds studied by Lagrangian particle tracking, *J. Atmos. Sci.*, *65*, 2581–2597, doi:10.1175/2008JAS2572.1.

Heus, T., H. J. J. Jonker, H. E. A. V. den Akker, E. J. Griffith, M. Koutek, and F. H. Post (2009), A statistical approach to the life cycle analysis of cumulus clouds selected in a virtual reality environment, *J. Geophys. Res.*, *114*, D06208, doi:10.1029/2008JD010917.

Kessler, E. (1969), *On the Distribution and Continuity of Water Substance in Atmospheric Circulations, Meteorol. Monogr. Ser.*, vol. 32, Am. Meteorol. Soc., Boston, Mass.

Khvorostyanov, V. I., and J. A. Curry (2002), Terminal fall velocities of droplets and crystals: Power laws with continuous parameters over the size spectrum, *J. Atmos. Sci.*, *59*, 1872–1884.

Khvorostyanov, V. I., and J. A. Curry (2005), Fall velocities of hydrometeors in the atmosphere: Refinements to a continuous analytical power law, *J. Atmos. Sci.*, *62*, 4343–4357.

Larsen, M. L., A. B. Kostinski, and A. R. Jameson (2014), Further evidence for superterminal raindrops, *Geophys. Res. Lett.*, *41*, 6914–6918, doi:10.1002/2014GL061397.

Low, T. B., and R. List (1982), Collision, coalescence and breakup of raindrops. Part I: Experimentally established coalescence efficiencies and fragment size distributions in breakup, *J. Atmos. Sci.*, *39*, 1591–1606.

Magaritz, L., M. Pinsky, O. Krasnov, and A. Khain (2009), Investigation of droplet size distributions and drizzle formation using a new trajectory ensemble model. Part II: Lucky parcels, *J. Atmos. Sci.*, *66*, 781–805.

Mansell, E. R. (2010), On sedimentation and advection in multimoment bulk microphysics, *J. Atmos. Sci.*, *67*, 3084–3094.

Marshall, J. S., and W. M. K. Palmer (1948), The distribution of raindrops with size, *J. Meteorol.*, *5*, 165–166.

Mason, B. J. (1971), *The Physics of Clouds*, 2nd ed., Oxford Univ. Press, Oxford, U. K.

Mazzitelli, I. M., F. Toschi, and A. S. Lanotte (2014), An accurate and efficient Lagrangian sub-grid model, *Phys. Fluids*, *26*, 095191.

Milbrandt, J., and R. McTaggart-Cowan (2010), Sedimentation-induced errors in bulk microphysics schemes, *J. Atmos. Sci.*, *67*, 3931–3948.

Milbrandt, J., and M. Yau (2005), A multimoment bulk microphysics parameterization. Part I: Analysis of the role of the spectral shape parameter, *J. Atmos. Sci.*, *62*, 3051–3064.

Montero-Martínez, G., A. B. Kostinski, R. A. Shaw, and F. García-García (2009), Do all raindrops fall at terminal speed?, *Geophys. Res. Lett.*, *36*, L11818, doi:10.1029/2008GL037111.

Pruppacher, H. R., and J. D. Klett (1997), *Microphysics of Clouds and Precipitation*, Kluwer Acad., Dordrecht, Netherlands.

Pruppacher, H. R., and R. Rasmussen (1979), A wind tunnel investigation of the rate of evaporation of large water drops falling at terminal velocity in air, *J. Atmos. Sci.*, *36*, 1255–1260.

Rangno, A. L. (2008), Fragmentation of freezing drops in shallow maritime frontal clouds, *J. Atmos. Sci.*, *65*(4), 1455–1466.

Rauber, R. M., et al. (2007), Rain in shallow cumulus over the ocean—The RICO campaign, *Bull. Am. Meteorol. Soc.*, *88*, 1912–1924, doi:10.1175/BAMS-88-12-1912.

Riechelmann, T., Y. Noh, and S. Raasch (2012), A new method for large-eddy simulations of clouds with Lagrangian droplets including the effects of turbulent collision, *New J. Phys.*, *14*, 065008, doi:10.1088/1367-2630/14/6/065008.

Rogers, R. R., and M. K. Yau (1989), *A Short Course in Cloud Physics, International Series in Natural Philosophy*, vol. 113, 3rd ed., Elsevier, Oxford, U. K.

Sant, V., U. Lohmann, and A. Seifert (2013), Performance of a triclass parameterization for the collision–coalescence process in shallow clouds, *J. Atmos. Sci.*, *70*(6), 1744–1767.

Savic-Jovcic, V., and B. Stevens (2008), The structure and mesoscale organization of precipitating stratocumulus, *J. Atmos. Sci.*, *65*, 1587–1605.

Seifert, A. (2008), On the parameterization of evaporation of raindrops as simulated by a one-dimensional rainshaft model, *J. Atmos. Sci.*, *65*, 3608–3619.

Seifert, A., and K. D. Beheng (2001), A double-moment parameterization for simulating autoconversion, accretion and selfcollection, *Atmos. Res.*, *59–60*, 265–281.

Seifert, A., and T. Heus (2013), Large-eddy simulation of organized precipitating trade wind cumulus clouds, *Atmos. Chem. Phys.*, *13*(1), 5631–5645, doi:10.5194/acp-13-5631-2013.

Seifert, A., A. Khain, U. Blahak, and K. D. Beheng (2005), Possible effects of collisional breakup on mixed-phase deep convection simulated by a spectral bin cloud model, *J. Atmos. Sci.*, *62*, 1917–1931.

Seifert, A., U. Blahak, and R. Buhr (2014), On the analytic approximation of bulk collision rates of non-spherical hydrometeors, *Geosci. Model Dev.*, 7, 463–478, doi:10.5194/gmd-7-463-2014.

Shima, S., K. Kusano, A. Kawano, T. Sugiyama, and S. Kawahara (2009), The super-droplet method for the numerical simulation of clouds and precipitation: A particle-based and probabilistic microphysics model coupled with a non-hydrostatic model, *Q. J. R. Meteorol. Soc.*, 135, 1307–1320, doi:10.1002/qj.441.

Sölch, I., and B. Kärcher (2010), A large-eddy model for cirrus clouds with explicit aerosol and ice microphysics and Lagrangian ice particle tracking, *Q. J. R. Meteorol. Soc.*, 136(B), 2074–2093.

Stevens, B. (2007), On the growth of layers of non-precipitating cumulus convection, *J. Atmos. Sci.*, 64, 2916–2931.

Stevens, B., and A. Seifert (2008), Understanding macrophysical outcomes of microphysical choices in simluations of shallow cumulus convection, *J. Meteorol. Soc. Jpn.*, 86, 143–162.

Stevens, B., R. Walko, and W. Cotton (1996), The spurious production of cloud-edge supersaturation by Eulerian models, *Mon. Weather Rev.*, 124, 1034–1041.

Stevens, B., C.-H. Moeng, and P. P. Sullivan (1999), Large-eddy simulations of radiatively driven convection: Sensitivities to representation of small scales, *J. Atmos. Sci.*, 56, 3963–3984.

Stevens, B., et al. (2005), Evaluation of large-eddy simulations via observations of nocturnal marine stratocumulus, *Mon. Weather Rev.*, 133, 1443–1462.

Straub, W., K. D. Beheng, A. Seifert, J. Schlottke, and B. Weigand (2010), Numerical investigation of collision-induced breakup of raindrops. Part II: Parameterizations of coalescence efficiencies and fragment size distributions, *J. Atmos. Sci.*, 67(3), 576–588.

Sutherland, W. (1893), The viscosity of gases and molecular force, *Philos. Mag.*, 5(36), 507–531.

van Zanten, M. C., et al. (2011), Controls on precipitation and cloudiness in simulations of trade-wind cumulus as observed during RICO, *J. Adv. Model. Earth Syst.*, 3, M06001, doi:10.1029/2011MS000056.

Wacker, U., and A. Seifert (2001), Evolution of rain water profiles resulting from pure sedimentation: Spectral vs. parameterized description, *Atmos. Res.*, 58, 19–39.

Wang, L. P., B. Rosa, H. Gao, G. He, and G. Jin (2009), Turbulent collision of inertial particles: Point-particle based, hybrid simulations and beyond. *Int. J. Multiphase Flow*, 35(9), 854–867.

Weil, J. C., P. P. Sullivan, and C.-H. Moeng (2004), The use of large-eddy simulations in Lagrangian particle dispersion models, *J. Atmos. Sci.*, 61, 2877–2887.

Yamaguchi, T., and D. A. Randall (2012), Cooling of entrained parcels in a large-eddy simulation, *J. Atmos. Sci.*, 69, 1118–1136, doi:10.1175/JAS-D-11-080.1.

Yang, Y., G.-W. He, and L.-P. Wang (2008), Effects of subgrid-scale modeling on Lagrangian statistics in Large-Eddy Simulation, *J. Turbulence*, 9, 1–24, doi:10.1080/14685240801905360.